World Scientific
www.worldscientific.com

FET THZ DETECTORS OPERATING IN THE QUANTUM CAPACITANCE LIMITED REGION

BERARDI SENSALE-RODRIGUEZ, LEI LIU, RONGHUA WANG, TOM ZIMMERMANN,
PATRICK FAY, DEBDEEP JENA and HUILI (GRACE) XING

Department of Electrical Engineering, University of Notre Dame, 275 Fitzpatrick Hall
Notre Dame, IN 46556, USA
bsensale@nd.edu and hxing@nd.edu

In this paper, we report our studies on field effect transistor (FET) THz detectors operating in the non-resonant mode based on the Dyakonov-Shur plasma wave detection theory, where the quantum capacitance dominates. The influence of quantum capacitance in detector response is theoretically developed and numerically simulated at low and high frequencies. Fundamental constraints in the upper frequency limit are also analyzed for FET THz detectors based on various materials, showing advantages of GaN for 8 - 20 THz applications. Experiments at microwave and THz frequencies have been carried out for GaN based devices showing agreement with the theory.

Keywords: quantum capacitance; THz detection; field effect devices; plasma wave; GaN; frequency limit.

1. Introduction

Dyakonov and Shur's theory [1-2] states that electrons in a high electron mobility transistor (HEMT) can be described by a hydrodynamic model; and that the resultant plasma waves have nonlinear properties that can be utilized for THz emission and detection. Field-effect-transistor (FET) detectors based on the Dyakonov-Shur 2-D electron fluid (2DEF) have been touted in the past decade as an attractive candidate for THz detection; very high responsivities have been predicted ($> 10^7$ V/W has been predicted assuming unity coupling efficiency of incident signal to device [1]; ~ 1000 V/W has been reported experimentally at 1.4 THz at RT working in the resonant regime [3]). This detection mechanism has been reported by various laboratories using Si [4], GaAs [5-8] and GaN [3, 9] FETs. However, it is not yet clear which semiconductor is the best choice for THz detection. In this work, we report our studies on the fundamental limits posed by the semiconductor itself as well as FET THz detectors operating in the non-resonant mode. Since the responsivity is predicted to peak near the FET threshold voltage for non-resonant detection, a model taking into account of quantum capacitance is developed to calculate detector responsivity.

This work is organized as follows. In Section 2 quantum capacitance is defined and its importance in relation to detector response near threshold voltage. In Section 3 various materials are compared for plasma wave detection at high frequencies, showing the

advantages of GaN over competing materials including Si, GaAs and InAs. In Section 4 and 5 our effort toward developing GaN HEMT based THz detectors are presented including the device structures and their responsivities under microwave and THz excitation.

2.   Effect of quantum capacitance in responsivity

When the FET detector operates in the non-resonant mode, the channel electron plasma wave, excited by the incoming electromagnetic wave, quickly damps under the gate from the source to drain. In this mode, its responsivity R has been predicted to be infinity at the FET threshold voltage using a highly simplified expression (channel sheet charge $n_s = 0$ at V_{th}) [1]. Analytical expression of R was also derived in the threshold region using a phenomenological exponential dependence of n_s on V_{gs} [9] but without explicitly considering the effect of quantum capacitance (QC), which is particularly important near V_{th} and provides more insight on the device physical picture. Here we express R rather rigorously as a function of n_s and dn_s/dV_{gs}, which calls for inclusion of quantum capacitance. An expression for responsivity as a function of frequency (ω) is given in Ref. [1]:

$$R = \frac{qV_a^2}{4Pm^*s^2} f\left(\omega, s\right) \ .$$ (1)

where $f\left(\omega, s\right)$ is given by:

$$f\left(\omega, s\right) = 1 + \frac{2\omega\tau}{\sqrt{1+\left(\omega\tau\right)^2}} - \frac{1}{\sqrt{1+\left(\omega\tau\right)^2}} \frac{\sqrt{1+\left(\omega\tau\right)^2} + 2\omega\tau\cos\left(2k_0^+L\right)}{\sinh^2\left(k_0^-L\right) + \cos^2\left(k_0^+L\right)} \ .$$ (2)

with:

$$k_0^\pm = \frac{\omega}{s}\left(\frac{\sqrt{1+\omega^{-2}\tau^{-2}}\pm 1}{2}\right)^{1/2} \ .$$ (3)

where m^* is electron conduction effective mass, τ is electron relaxation time, s the velocity of the plasma waves, V_a the external microwave voltage between gate and source, and P is the available microwave power. Based on this analysis, a comparative study of Si FETs and AlN/GaN HEMTs with submicron gate lengths is presented below, both of which have been touted suitable for THz detection. Responsivities of both FETs have been numerically simulated and compared at low and high frequencies since the two materials exhibit comparable m^* but different 2DEG mobility in the highly scaled FETs.

Near V_{th} one can assume a band diagram under the gate with quantized energy levels in the channel [10], which is applicable to GaN HEMTs and Si submicron FETs due to the high transverse electric field in the channel near V_{th}. Considering this, charge in the channel can be expressed as:

$$n_s(E_f) = \sum_i \int_{E_i}^{\infty} DOS.f(E)dE.$$ (4)

where $i=1...M$ with M being the number of quantized energy levels, and *DOS* is the 2D density of states, which is given by:

$$DOS = m^*_{DOS} / \pi \hbar^2.$$ (5)

with m^*_{DOS} being the 2D *DOS* electron effective mass. Taking into account the Fermi-Dirac distribution, quantum capacitance (C_q) near V_{th} as a function of channel concentration (n_s) can be derived by assuming a single band occupation:

$$C_q = q^2 (g_v m^*_{DOS} / \pi\hbar^2)\left(1 - \exp\left(-n_s \pi\hbar^2 / kTm^*_{DOS}\right)\right).$$ (6)

Total capacitance can be written as: $C_{total} = (C_{gate}^{-1} + C_q^{-1})^{-1}$ and thus the plasma wave velocity *s* is given by:

$$s^2 = q^2 n_s / m^* C_{total}.$$ (7)

where C_{total} is a function of n_s as can be seen from (6).

Shown in Fig. 1 are simulated responsivities for Si FETs and AlN/GaN HEMTs as a function of n_s for different frequencies using the above expressions; quantum capacitance, total capacitance, plasma wave velocity and responsivity are also plotted. The material parameters and transistor dimensions used for this simulation are: EOT = 5 nm, L = 150 nm; Si FET μ = 300 cm^2/Vs, g_v = 2, m^*_{DOS} = 0.19m$_0$ (<100> surface orientation) [11]; AlN/GaN HEMT, μ = 1500 cm^2/Vs, g_v = 1, m^*_{DOS} = 0.2m$_0$. The detector responsivity maximizes near V_{th} but being finite, where the quantum capacitance dominates. This trend is consistent with Ref. [9]. Even though a slightly higher EOT was assumed in this exercise interesting observations can still be made since the material parameters have been used: at low frequencies, the maximum responsivity is inversely proportional to electron mobility; while at high frequencies, it is proportional to mobility (below 200 GHz, *R* of the Si FET is greater than that of the GaN HEMT; while above the opposite occurs, and the peaks at high n_s indicate resonant mode operation). This analysis shows that AlN/GaN HEMTs promise a greater *R* at high frequencies (> 200 GHz) in the non-resonant mode near the quantum capacitance limited region compared to highly scaled Si FETs.
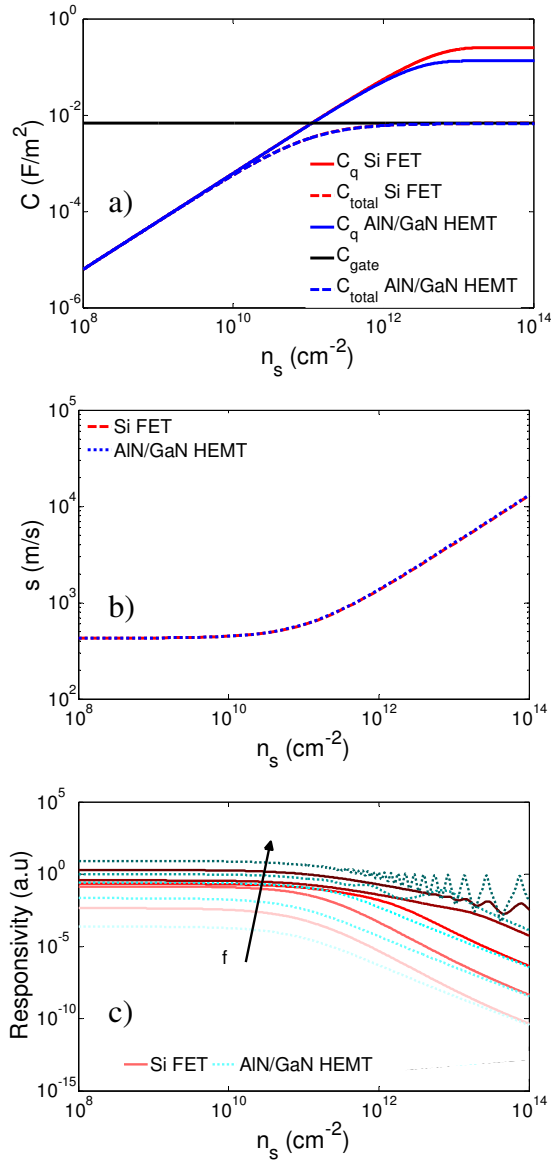
Fig. 1. (a) Capacitances, (b) electron plasma wave velocity, and (c) responsivity (f = [2, 20, 200, 2000, 20000] GHz); as a function of channel concentration.

3. Upper frequency limit

Many applications, such as detection and identification of certain explosives, require detectors exhibiting high frequency operation (e.g. Tetryl absorption peaks are located at 5.97 and 10.11 THz) [12]. As discussed above at high frequencies the 2DEF-based detectors with high channel carrier mobilities exhibit high responsivities. It is then

expected that narrow bandgap semiconductor FETs with high carrier mobility channels (e.g., InAs) should outperform wide bandgap FETs, such as GaN. But, in what frequency range does this hold? Which material promises higher frequency operation? In this section we will argue that GaN based devices have unique advantages in operation frequencies higher than 7 THz. There are two distinct effects that affect the high frequency behavior of these detectors: i) plasmon and optical phonon coupling, and ii) maximum achievable 2-D carrier concentration $n_{s,max}$. While the effect of phonons is common to both resonant and non-resonant modes of detection [13], $n_{s,max}$ is particularly important when considering resonant detection, where detection frequency depends on channel charge density [1, 14-15]. The expression for plasmon frequency in 2D systems is [14]:

$$f = \frac{1}{2\pi}\sqrt{\frac{q^2 n_s k}{2\varepsilon_0 \varepsilon_\infty m^*}} \; . \tag{8}$$

where ε_0 is the permittivity of vacuum, ε_∞ is the high frequency dielectric constant of the semiconductor, and k is the wave vector in the 2DEG, which can be replaced by the Fermi vector k_f:

$$k_f = \sqrt{2\pi n_s} \; . \tag{9}$$

Equations (8)-(9) show how plasma frequency is limited by the maximum achievable 2-D carrier concentration, a property of the FET material system. Listed in Table 1 are the typical values of $n_{s,max}$ in 2DEF devices and the corresponding maximum plasmon frequency achievable. Also listed in Table 1 are Restrahlen band energies (between the transverse optical (TO) and longitudinal optical (LO) phonon energies) of Si, GaN, GaAs, InAs [16] and graphene [17], and their correspondent associated frequencies and wavelengths. Electromagnetic waves in the Restrahlen band cannot propagate in a material due to the strong interaction between photons and phonons. Similarly, a strong plasmon-phonon coupling is expected in this energy range thus the corresponding plasmon modes are forbidden. Plasmons with energy above Restrahlen bands most likely suffer from strong scattering with LO phonons, similar to the case for electrons. As a result, the maximum allowed plasmon frequency in these 2DEF FETs is the lower of the two aforementioned effects, thus setting the fundamental upper operation frequency of the 2DEF-based THz detectors. It can be seen in the table that the maximum plasmon frequency allowed by $n_{s,max}$ is always higher than that due to plasmon-phonon coupling. For instance, the upper frequency limit for GaN is 16 THz, while for GaAs and InAs is much lower, ~ 7 THz, due to their low TO/LO phonon energies. Graphene is also a very interesting material for THz applications since its LO phonon energy is the highest. However, the biggest challenge at present is how to harvest the intrinsic high mobility

nature of graphene in a realistic device layout. Out of today's common semiconductors, GaN is most attractive for 2DEF THz detectors in the frequency range of 7 - 16 THz from this point of view.

Table 1. LO phonon energy and correspondent frequency for several materials.

Material	i) Restrahlen band (TO - LO phonon energy) (meV)	i) Associated freq. (THz) & wavelength (um)	ii) Typical $n_{s,max}$ (cm^{-2})	ii) Associated freq. (THz) & wavelength (um)	Max. operating freq. (THz)
Si	57-63	13.9-15.5 / 20-22	2×10^{13}	62 / 5	14
GaN	66-92	16-22 / 19-22	3×10^{13}	92 / 3	16
GaAs	31-36	7.5-8.5 / 34-40	5×10^{12}	36 / 8	7.5
InAs	27-29	6.4-7.0 / 43-46	2×10^{12}	28 / 11	6.4
Graphene	160	38.6 / 8	5×10^{13}	-	38.6

4. AlN/GaN HEMT devices

In the aforementioned arguments we have shown that GaN-based FET THz detectors are attractive for their reasonably high channel carrier mobility and promising high frequency operation. Next we report our initial effort in demonstrating GaN FETs for THz detection in the quantum-capacitance limited region (non-resonant detection), the AlN/GaN HEMTs used in the study have been originally developed for high speed high power transistors [10, 18-20]. Three types of AlN/GaN HEMTs were investigated: AlN/GaN depletion mode, InAlN/AlN/GaN depletion-mode with no gate recess and enhancement-mode devices with gate recessed to AlN barrier on the same wafer. The InAlN/AlN/GaN HEMTs were grown by IQE RF LLC and processed at Triquint semiconductor (HEMT A and B), and more details on device fabrication and performance can be found in Ref. [10, 20]; The AlN/GaN D-mode devices (HEMT C) were grown and fabricated at the University of Notre Dame, and more details on growth and fabrication can be found in Ref. [21].

The schematic of the device structures is illustrated in Fig. 2. The device parameters are as follows (with the 2DEG properties derived from either the Hall effect measurement
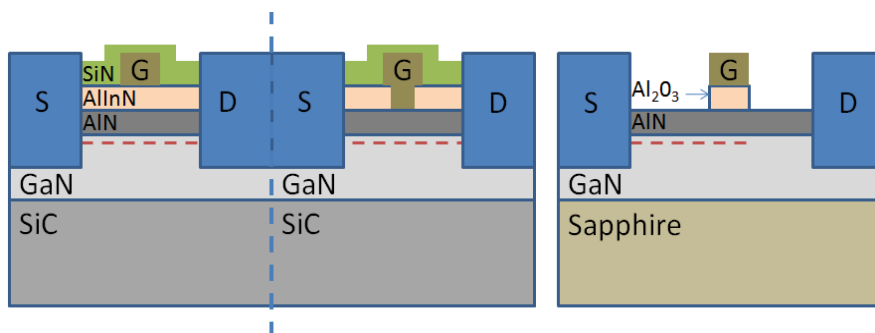

Fig. 2. Schematic of the device structures (a) D-mode HEMT A; (b) E-mode HEMT B; (c) D-mode HEMT C.

or the HEMT I-Vs). HEMT A: D-mode, L_g = 150 nm, W = 50 µm, $n_s \sim$ 2 x 10^{13} cm^{-2} and $\mu \sim$ 1400 cm^2/V.s; HEMT B: E-mode, L_g = 150 nm, W = 400 µm, $\mu \sim$ 1000 cm^2/V.s is estimated for $n_s \sim$ 1.75 x 10^{13} cm^{-2} and; HEMT C: D-mode, L_g = 2 µm, W = 25 µm, $n_s \sim$ 2 x 10^{13} cm^{-2} and $\mu \sim$ 1300 cm^2/V.s. The device DC transfer curves at V_{ds} = 0.05 V are presented in Fig. 3. V_{th} is determined by the linear extrapolation of I_d in the transfer curve. It is important to notice that HEMT A and B exhibited small gate leakage currents
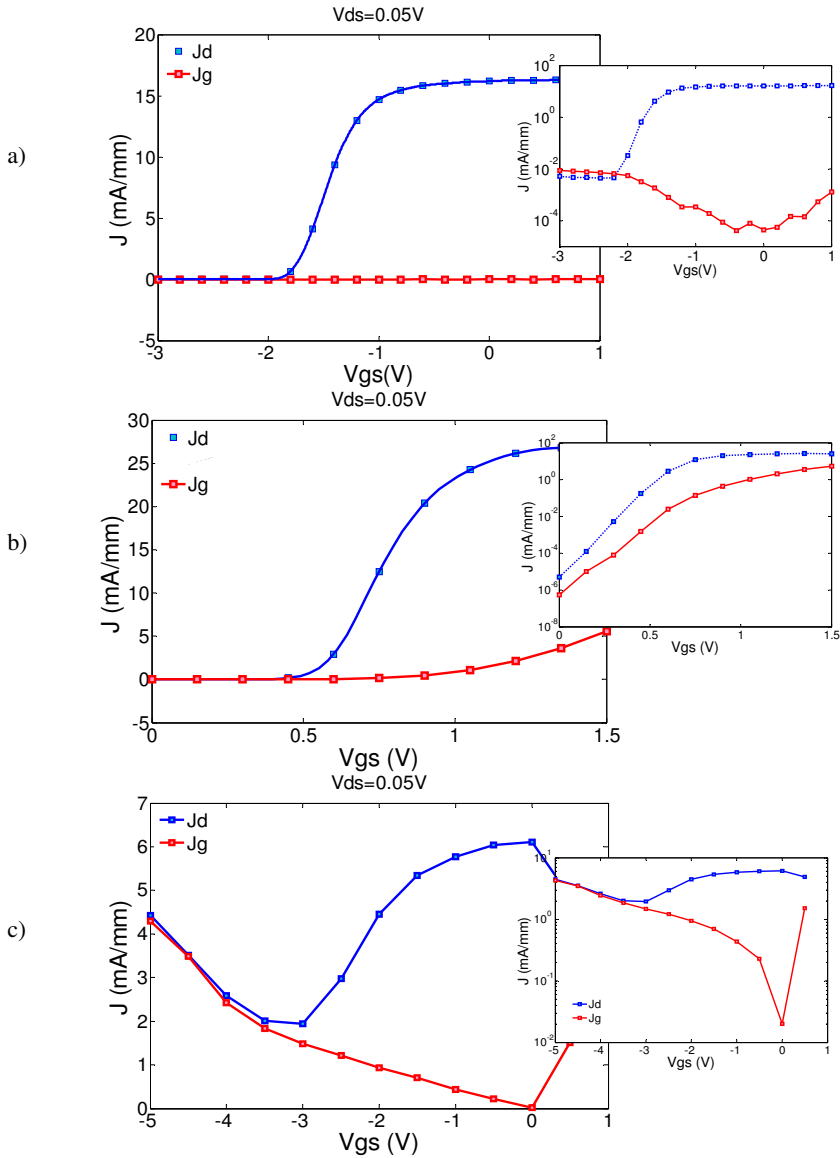
Fig. 3. DC transfer curves (a) HEMT A, (b) HEMT B, (c) HEMT C.

(I_g more than one order of magnitude smaller than I_d near V_{th}) , while HEMT C suffered from high gate and buffer leakage. In the case of non resonant detection, low gate leakage is essential for a 2DEF THz detector to operate in the deep pinch-off (i.e. quantum capacitance) region, where maximal responsivity is expected. As will be shown in the next section's microwave measurements a high gate leakage results in degraded detector performance.

5. Microwave and THz measurements

Microwave measurements (up to 45 GHz) were performed at room temperature on HEMT A and HEMT C. The microwave measurement setup is presented in Fig. 4. The output RF power from the VNA (*P0*) was fixed at -10 dBm, and the detector responsivity, was calculated as $R = V_{ds} / P_{in}$, where P_{in} is the power delivered to the device after correcting for the cable loss and reflection based on the reflection measurement (S11) at Port 1.
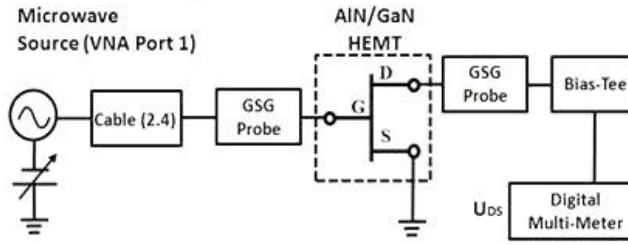

Fig. 4. Microwave measurement setup.

In the microwave frequency region expanding Eq. (2) in its Taylor series near $\omega \sim 0$ (assuming a constant plasmon velocity *s*), it can be seen that the dependence of responsivity R on frequency f is roughly quadratic (see also [22]). In addition, as it was presented on Fig. 1 (c), R is expected to maximize near or below threshold voltage, where the quantum capacitance dominates, and to decrease with increasing V_{gs} (i.e. n_s). The microwave measurement results on HEMT A are shown in Fig. 5 with the measured R values at different bias voltages in dots and the calculated parabolic trends in dashed lines. The relatively large noise in the measured R mainly stems from fluctuation of the RF signal output power from the VNA and manual recording of V_{DS}. It was indeed observed that the device R increases with $f^{\ 2}$ and decreases with increasing V_{gs} as predicted, indicating the device most likely operates in the non-resonant mode.

As already mentioned previously, low gate leakage is necessary to drive devices into deep sub-threshold region for improved responsivity (see Fig. 1 (c) and also [9, 19]). We have investigated experimentally the influence of leakage current on R by comparing HEMT A and C, and the results are shown in Fig. 6. The upper plot shows the normalized measured responsivity R at 35 GHz versus the gate drive V_{gs}-V_{th}, for both

HEMTs. R of HEMT A peaks near V_{th} as expected. However, R of HEMT C peaks around 2 V above V_{th} since the gate leakage is too high for gate drive < 2 V; with lower gate leakage the device responsivity should have kept increasing when approaching V_{th}. The lower plot shows the drain-gate current ratio in both devices, and it is observed that the responsivity of both devices peaks near $I_d/I_{gate} = 10$.
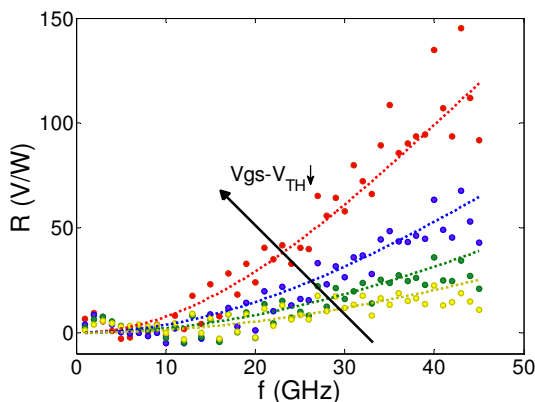

Fig. 5. Measured responsivity as a function of frequency for HEMT A at different bias voltages (V_{gs}-V_{TH} = [0.01 - 0.3] V, $P0$ = -10 dBm).
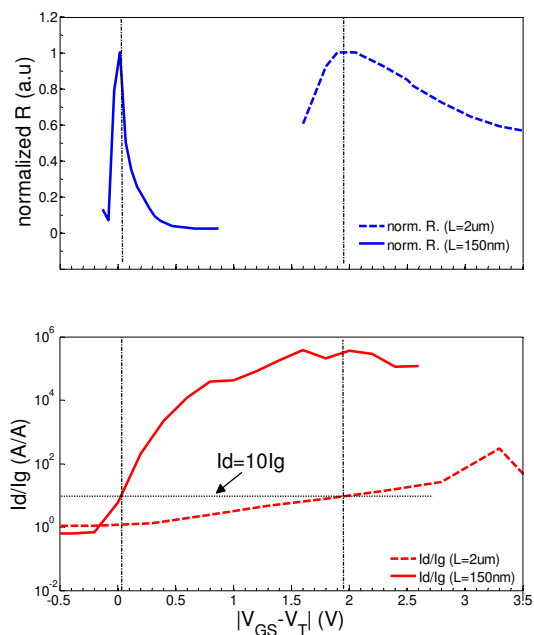

Fig. 6. Normalized R at 35 GHz (upper) and drain-gate current ratio vs. gate bias (lower) for HEMT A (solid) and HEMT C (dashed).
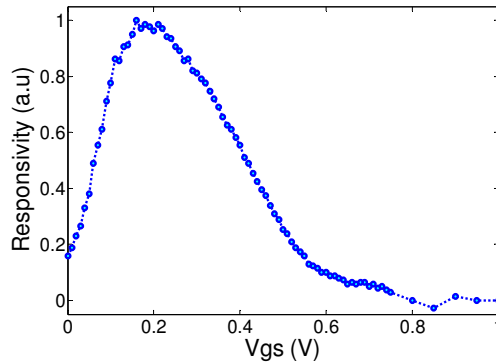
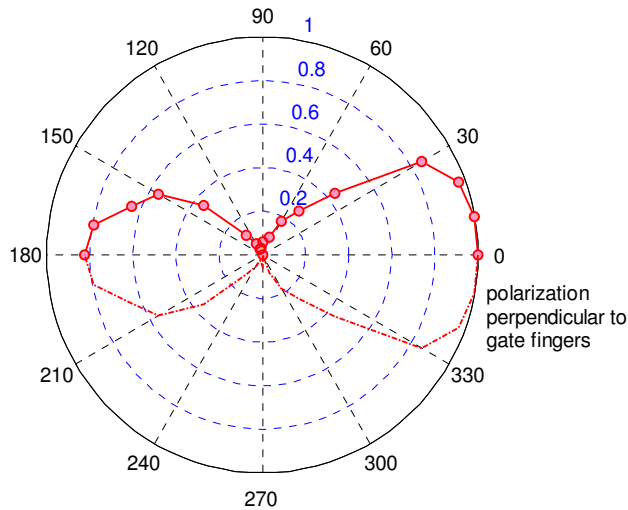Fig. 7. Responsivity as a function of gate bias for HEMT B at 610 GHz.

Fig. 8. Responsivity as a function of polarization angle (HEMT B).

THz measurements were performed on HEMT B at 610 GHz using a VDI (Virginia Diodes, Inc.) solid-state source. Radiation was directed in air onto the device, a variable power supply was used to provide the gate-source bias and the DC response was measured with a digital multi-meter. The measured responsivity is plotted in arbitrary units since THz signal coupling into the device needs yet to be studied. Fig. 7 shows the measured responsivity versus gate-source voltage, which also agrees well with the aforementioned trend: R is small for voltages much smaller than threshold (where the effect of leakage current is significant), peaks slightly below V_{th} (where the transistor is in the quantum capacitance limited region) and then decreases with increasing V_{gs}.

The device responsivity was also measured against polarization angle by rotating the device (Fig. 8). Maximum in R was observed when the polarization of the incoming THz

beam is perpendicular to the gate fingers. The asymmetry of this characteristic with respect to the vertical axis is attributed to the asymmetry of the contact structure [22]; measured data is presented in red dots, while the dashed curve is extrapolated from the symmetry of the device and contact structure with respect to the horizontal axis. Sakowicz et al. [23] reported the similar polarization dependence and asymmetry in a study to investigate mechanism of radiation coupling to plasma wave field effect transistor sub-THz detectors. The authors attributed this polarization dependence to the antenna effect of the device contact layout and bonding wires, which is probably the case in this study as well.

6. Conclusions

We have investigated the influence of quantum capacitance on the responsivity of 2-D electron fluid based microwave/THz detectors. In the quantum capacitance limited region, the 2DEF detector responsivity maximizes near V_{th} when operating in the non-resonant mode. Our study also shows that at low frequencies, R is inversely proportional to the electron channel mobility; while at high frequencies, R is proportional to the electron mobility. We compared the frequency limit of operation for different materials and showed the advantages of GaN based devices operating at high frequency range (> 7 THz). Motivated by these theoretical considerations, we investigated experimentally AlN/GaN HEMTs based THz detectors. Responsivity of AlN/GaN HEMTs was measured at room temperature at microwave frequencies (0.1-45 GHz) using a VNA and also at 610 GHz using a solid-state source, showing reasonable agreement with the theory. Future investigations focus on understanding unique features of plasmon induced nonlinearity in a 2DEF based THz detector as well as radiation coupling.

Acknowledgements

References

1. M. Dyakonov and M. S. Shur , *Detection, mixing, and frequency multiplication of terahertz radiation by two-dimensional electronic fluid*, IEEE Trans. Electron Devices **43**(3), 380-387 (1996).
2. M. Dyakonov and M. S. Shur, *Shallow water analogy for a ballistic field effect transistor: New mechanism of plasma wave generation by dc current*, Phys. Rev. Lett. **71**(15), 2465–2468 (1993).
3. T. Tanigawa, T. Onishi, S. Takigawa and T. Otsuji, *Enhanced Responsivity in a Novel AlGaN / GaN Plasmon-Resonant Terahertz Detector Using Gate-Dipole Antenna with Parasitic Elements*, Device Res. Conf. (DRC), 2010.
4. R. Tauk, F. Teppe, S. Boubanga, D. Coquillat, W. Knap, Y. M. Meziani, C. Gallon, F. Boeuf, T. Skotnicki, C. Fenouillet-Beranger, D. K. Maude, S. Rumyantsev, and M. S. Shur, *Plasma*

wave detection of terahertz radiation by silicon field effects transistors: Responsivity and noise equivalent power, Appl. Phys. Lett. **89**(25), 253 511-1–253 511-3 (2006).

5. W. Knap, Y. Deng, S. Rumyantsev, and M. S. Shur, *Resonant detection of subterahertz and terahertz radiation by plasma waves in submicron field-effect transistors*, J. Appl. Phys. Lett. **81**, 4637 (2002).

6. A. V. Antonov, V. I. Gavrilenko, E. V. Demidov, S. V. Morozov, A. A. Dubinov, J. Lusakowski, W. Knap, N. Dyakonova, E. Kaminska, A. Piotrowska, K. Golaszewska, and M. S. Shur, *Electron transport and terahertz radiation detection in submicrometer-sized GaAs/AlGaAs field effect transistors with two- dimensional electron gas*, Phys. Solid State **46**(1), 146–149 (2004).

7. F. Teppe, D. Veksler, V. Y. Kachorovski, A. P. Dmitriev, X. Xie, X.-C. Zhang, S. Rumyantsev, W. Knap, and M. S. Shur, *Plasma wave resonant detection of femtosecond pulsed terahertz radiation by a nanometer field effect transistor*, Appl. Phys. Lett. **87**(2), 022 102-1–022 102-3 (2005).

8. Elkhatib, T.A.; Kachorovskii, V.Y.; Stillman, W.J.; Veksler, D.B.; Salama, K.N.; Xi-Cheng Zhang; Shur, M.S.; , *Enhanced Plasma Wave Detection of Terahertz Radiation Using Multiple High Electron-Mobility Transistors Connected in Series*, IEEE Trans. Microwave Theory Tech. **58**(2), 331-339 (2010).

9. W. Knap, V. Kachorovskii, Y. Deng, S. Rumyantsev, J.-Q. Lu, R. Gaska, M. S. Shur, G. Simin, X. Hu, M. A. Khan, C. A. Saylor, and L. C. Brunel, *Nonresonant detection of terahertz radiation in field effect transistors*, J. Appl. Phys. **91**(11), 9346–9353 (2002).

10. R. Wang, P. Sanier, X. Xing, C. Lian, X. Gao, S. Guo, G. Snider, P. Fay, D. Jena, and H. G. Xing, *Gate-Recessed Enhancement-Mode InAlN/AlN/GaN HEMTs With 1.9-A/mm Drain-Current Density and 800-mS/mm Transconductance*, IEEE Electron Device Lett. **31**(12), in press (2010).

11. T. Janik and B. Majkusiak, *Analysis of the MOS Transistor Based on the Self-Consistent Solution to the Schrodinger and Poisson Equations and on the Local Mobility Model,* IEEE Trans. Electron Devices **45**(6), 1263-1271 (1998).

12. H. B. Liu, H. Zong, N. Karpowicz, Y. Chen, X. C. Zhang, *Terahetrz Spectroscopy and Imaging for Defense and Security Applications*, Proc. IEEE, **95**(8), 1514 (2007).

13. Y. Deng, Novel Solid State Terahertz Detectors and Emitters, PhD Thesis, Rensselaer Polytechnic Institute (2003).

14. Y. Cao and D. Jena, *Ultrathin AlN/GaN Heterojunctions by MBE for THz Applications,* Proc. Mater. Res. Soc. Symp., vol. 955 (2007).

15. L. Liu, B. Sensale-Rodriguez, Z. Zhang, T. Zimmermann, Y. Cao, D. Jena, P. Fay, and H. Xing, *Development of Microwave and Terahertz Detectors Utilizing AlN/GaN High Electron Mobility Transistors*, 21st Int. Symp. Space THz Tech. (ISSTT), 2010.

16. NSM Archive-Physical Properties of Semiconductors. Ioffe Institute; see http://www.ioffe.ru/SVA/NSM/Semicond/index.html.

17. T. Ando, *The electronic properties of graphene and carbon nanotubes*, NPG Asia Mater. **1**(1) 17–21 (2009).

18. D. Deen, T. Zimmermann, Y. Cao, D. Jena, and H. G. Xing, *2.3 nm AlN/GaN high electron mobility transistors with insulated gates*, Phys. Solid. Stat. (c), **5**(6), 2047 (2008).

19. B. Sensale-Rodriguez, L. Liu, Z. Zhang, P. Saunier, T. Zimmermann, Y. Cao, D. Jena, P. Fay and H. G. Xing*, Initial Studies on Microwave and Terahertz Detection Using AlN/GaN HEMTs*, Electronic Mat. Conf. (EMC), 2010.

20. Y. Tang, P. Saunier, R. Wang, A. Ketterson, X. Gao, S. Guo, G. Snider, D. Jena, H. Grace Xing, and P. Fay, *High-Performance Monolithically-Integrated E/D Mode InAlN/AlN/GaN HEMTs for Mixed-Signal Applications*, Int. Electron Dev. Meeting (IEDM), 2010.

21. T. Zimmermann, D. Deen, Y. Cao, J. Simon, P. Fay, D. Jena, and H. G. Xing, *AlN/GaN insulated gate HEMTs with 2.3 A/mm output current and 480 mS/mm transconductance*, IEEE Electron. Device Lett. **29**(7), 661-664 (2008).
22. R. M. Weikle, II, J.-Q. Lü, M. S. Shur, and M. I. Dyakonov, *Detection of microwave radiation by electronic fluid in high electron mobility transistors*, Electron. Lett. **32**(23), 2148-2149 (1996).
23. M. Sakowicz, J. Lusakowski, K. Karpierza and M. Grynberg, *Mechanism of Radiation Coupling to Plasma Wave Field Effect Transistor Sub-THz Detectors*, Acta Physica Polonica A. **114**(5), 1337-1342 (2008).